International Immunopharmacology 74 (2019) 105703

Contents lists available at ScienceDirect

International Immunopharmacology

journal homepage: www.elsevier.com/locate/intimp

Berberine coated mannosylated liposomes curtail RANKL stimulated osteoclastogenesis through the modulation of GSK3β pathway via upregulating miR-23a

Sali Sujitha, Mahaboobkhan Rasool*

Immunopathology Lab, School of Bio Sciences and Technology, VIT, Vellore 632014, Tamil Nadu, India

ARTICLE INFO

Keywords:
Rheumatoid arthritis
ML-BBR
miR-23a
GSK3β/p-GSK3β
Osteoclastogenesis

ABSTRACT

Drug-induced microRNAs manifest significant therapeutic approaches; however, such progress in the treatment of osteopathic disorders including osteoporosis and rheumatoid arthritis still remains obscure. Contrarily, non-specific drug delivery, at high doses, increases the risk of side effects and reduces drug therapeutic efficacy. Accordingly, the present study was designed to examine the therapeutic effect of berberine coated mannosylated liposomes (ML-BBR) on RANKL (100 ng/ml) stimulated bone marrow-derived monocytes/macrophages (BMMs) via altering miR-23a expression. Initial studies using confocal microscopy showed successful internalization of ML-BBR in RANKL stimulated BMMs. Treatment with ML-BBR abrogated the increased osteoclast formation in BMM cells via inhibiting phosphorylated glutathione synthase kinase beta (p-GSK3β) mediated NFATc1 activation. Consequently, ML-BBR also attenuated the expression of bone-degrading enzymes (TRAP, cathepsin K and MMP-9) thereby inhibiting the bone resorptive activity of osteoclasts. Moreover, ML-BBR induced the expression levels of miR-23a at the gene level, which in turn attenuated GSK3β/p-GSK3β expression as confirmed via blotting analysis. Further miR-23a inhibition of the GSK3β phosphorylation was confirmed using luciferase reporter assay. Comparatively, LY2090314 (GSK3β inhibitor) treatment inhibited the protein level expression of GSK3β/p-GSK3β. However, LY2090314 treatment induced a basal level expression of miR-23a owing to the suggestion that ML-BBR has an influential role in upregulating miR-23a level to inhibit GSK-3β phosphorylation. Cumulatively, our findings endorsed that preferential internalization of ML-BBR by BMMs effectively modulated the RANKL/p-GSK3β pathway and curtailed the osteoclast-mediated bone erosion possibly through post-transcriptional gene silencing via miR-23a.

1. Introduction

Bone remodeling is a crucial cellular phenomenon involved in the development and maintenance of lifelong skeletal homeostasis. However, in several pathological states like rheumatoid arthritis, the bone erosion and formation event underpinning joint integrity creates a further imbalance leading to significant deformity in the bone morphology resulting in serious disability and poor functional outcome [1]. Increased bone resorption is generally attributed to enhanced production of several pro-inflammatory cytokines and receptor activator of nuclear factor κB ligand (RANKL) in particular [2,3]. Indeed, the amplified productions of these pro-inflammatory mediators drive the activation of bone-resorbing osteoclast cells thereby perpetuating the bone loss.

Osteoclasts, which are the large multi-nucleated bone-eating cells, play a unique role in dissolving the bone matrix components during the bone remodeling process. Howbeit, the number and functional activity of osteoclasts increases in several clinical disorders associated with aberrant bone loss. Osteoclast differentiation and activation, via the process of osteoclastogenesis, is controlled by stimulation with macrophage colony-stimulating factor (MCSF) and RANKL, the crucial osteoclastogenic factors. [4,5]. As a result, RANKL interacts with its cognate receptor RANK expressed on osteoclast precursor cells and activates the NFATc1, the transcription factor which ultimately facilitates the terminal differentiation and activation of the osteoclasts [6]. Activated osteoclast, in turn, releases bone degradative enzymes (TRAP, cathepsin K, MMP-9) that actively resorb the bone [7]. More importantly, RANKL priming of osteoclast precursors has been considered to be an obvious pathway that majorly aggravates the process of osteoclastogenesis. To compound the importance of RANKL further,

* Corresponding author at: SMV 240, Immunopathology Lab, School of Bio Sciences and Technology, VIT, Vellore 632 014, Tamil Nadu, India.
E-mail address: rasool.m@vit.ac.in (M. Rasool).

https://doi.org/10.1016/j.intimp.2019.105703
Received 29 April 2019; Received in revised form 12 June 2019; Accepted 13 June 2019
Available online 28 June 2019
1567-5769/

studies have proposed that RANKL is potentially responsible for the multistep development process of osteoclasts; including its migration, fusion, and activation [8]. In contrast, in vivo studies have shown that knockout mice deficient for RANKL attenuated osteoclastogenesis therein concluding the essential role of RANKL in osteoclast-mediated bone degradation. [9]. Therefore, it is necessary to explore new therapeutic avenues that can target RANKL activated downstream signaling pathways to prevent osteoclast related bone disorders.

Multiple signaling pathways like NF-κB, MAPKs (ERK, JNK, p38), PI3K/AKT and Wnt signaling are activated downstream of the RANKL stimulation [10–12]. Nevertheless, recent reports have highlighted that RANKL mediated GSK3β/NFATc1 pathway plays a crucial role in the process of osteoclast differentiation and function [13,14]. Importantly, it has been reported that RANKL mediated p-GSK3β (S9 phosphorylation) upregulation promotes osteoclastogenesis in bone marrow-derived monocyte/macrophages [13]. Additionally, GSK3β possesses multiple regulatory effects on inflammation via NF-κB signaling pathway [15]. In line with this report, it has been shown that GSK3β inhibition ameliorates the renal expression levels of RANK, RANKL, and NF-κB in a rat model of diabetic nephropathy, a type of inflammatory process associated with diabetic mellitus [16]. Moreover, PI3K/Akt mediated NFATc1 induction via p-GSK3β plays an important role in RANKL-induced osteoclastogenesis suggesting the indispensable role of GSK3β/NFATc1 axis in osteoclast differentiation [14]. Another study demonstrated that PKCβ controls the activity of NFATc1 by inactivating GSK-3β, thereby resulting in multi-nucleation and bone resorption function of osteoclasts [17]. Furthermore, transgenic mice overexpressing a constitutive active mutant of GSK-3β exhibited a marked reduction in the number of osteoclasts in vivo, as well as impaired osteoclast formation in vitro [13]. Frequent studies have also demonstrated the aberrant activation of non-canonical Wnt signaling (GSK3β/CaN/NFATc1) in the disruption of knee-joint homeostasis [11,18]. GSK3β inhibition also suppresses osteolysis by regulating both osteoblast and osteoclast differentiation in a rat model of instability-induced osteolysis [19]. Accordingly, uncovering the potential therapeutics that can manipulate GSK3β/NFATc1 pathway mediating osteoclastogenesis will pave way for effective clinical implications.

Current therapies prescribed against the management of inflammatory bone diseases include small molecular inhibitor, anti-RANKL monoclonal antibody (denosumab) and clinical drugs for osteoporosis such as bisphosphonates, estrogen, and calcitonin [20,21]. However, due to the low bioavailability, high clearance rate, and limited selectivity, patients require high and frequent dosage to attain sufficient therapeutic efficacy which can result in several disadvantages. As an alternative to the current treatment, plant derivatives, which are novel inhibitors of several inflammatory pathways, manifest minimal or no side effects and have been utilized frequently as therapeutics in recent times [22]. On this premise, we decided to investigate the effect of berberine (BBR), a Chinese herbal medicine that has been currently identified to be a potential candidate for therapeutic targeting of various cancers, type II diabetes mellitus and RA [23,24]. The potential role of BBR in inhibiting RANKL-mediated osteoclast differentiation and consequent joint destruction in a zymosan-induced mouse model of erosive arthritis has been reported [25]. Interestingly, it has also been reported that BBR has the potential for ameliorating hyperglycemia via inhibiting the phosphorylated GSK3β levels in diabetic mice model [26]. However, presently, no study has reported the therapeutic efficacy of BBR on RANKL stimulated GSK3β/NFATc1 mediated osteoclastogenesis and bone erosion. Successful inhibition of these parameters by BBR further requires the elucidation of detailed molecular mechanism, which remains unknown.

Among the various factors regulating bone erosion, miRNA dysregulation also majorly contributes to disease severity especially by modulating the unique network of bone homeostasis. In a study, miR-146a deficiency in arthritic synovial fibroblasts increased joint destruction specifically via unbalancing major regulatory factors like RANKL and osteoprotegerin (OPG), a decoy receptor of RANKL in TNF-driven model of arthritis [9]. Likewise, upregulation of miR145 inhibited the expression of Smad3, a positive regulator of RANKL-induced osteoclastogenesis [27]. Other microRNAs such as miR-17/20a, miR-124, and miR-7b are reported in regulating osteoclastogenesis by reducing NFATc1 expression and thereby unraveling major role in skeletal remodeling [28–30]. Decisively, it has been suggested that the regulation of miRNAs level by bioactive compounds could be a promising therapeutic strategy in preventing bone erosion associated with osteopathic disorders. BBR, a potential activator of several miRNAs has been explored in various cancer models that can suppress uncontrolled cell growth and proliferation [23,31]. Moreover, the anti-hepatocellular carcinoma effect of berberine through the upregulation of miR-23a has also been reported [31]. Recently, it has been depicted that miR-23a selectively inhibits the activation of IKKα in IL-17 stimulated chondrocytes model of RA [32].

Multiple studies have reported that the liposomal drug carriers incorporated with dexamethasone palmitate and methotrexate are effective in arthritic rat models [33,34]. Further, immunogenicity, biocompatibility, and non- toxic liposomal formulations have been proven to be a well-approved drug carrier system in several disease models. Contrastingly, clodronate containing liposomal therapy focused on synovial macrophages failed due to their interaction with macrophages in the liver and spleen instead of counteracting with macrophages in the synovial lining only and thereby resulted in their massive depletion [35]. However, this is not an appreciable approach since macrophages have a pivotal role in immune surveillance. At this scenario, selective targeting of activated macrophages is inevitable. Therefore, in our present study, berberine encapsulated mannosylated liposomes (ML-BBR) were synthesized to specifically target RANKL stimulated bone marrow macrophages. The drug-loaded liposomes were coated with mannose ligands for its preferential internalization and enhanced in vivo uptake by differentiated macrophages that express elevated levels of mannose receptors [36]. Our focus is thus to evaluate whether ML-BBR is able to ameliorate the osteoclast-mediated bone erosion via RANKL/GSK3β pathway through the activation/upregulation of miR-23a levels.

2. Materials and methods

2.1. Reagents

Berberine, 1, 2-Distearoyl-Sn-glycero-3-phosphocholine (DSPC), cholesterol, *p*-aminophenyl-D-mannopyranoside (mannose) and dialysis membrane were purchased from Sigma Chemicals (St. Louis, MO, USA). Dulbecco's modified Eagle's medium (DMEM), fetal bovine serum (FBS), trypsin and antibiotics (penicillin and streptomycin) were obtained from HIMEDIA (Mumbai, India). N-(Fluorescein-5-Thiocarbamoyl)-1, 2-Dihexadecanoyl-sn-Glycero-phosphoethanolamine Triethylammonium Salt (F-DHPE) was supplied by Invitrogen, (Massachusetts, USA). Recombinant RANKL and M-CSF were supplied by PeproTech (Rocky Hill, USA). High capacity cDNA reverse transcriptase kit was purchased from Applied Biosystems (Foster City, NY, USA) and EvaGreen mastermix was purchased from G-Biosciences (St. Louis, MO, USA). Transfection reagent (Xfect^{TM} RNA transfection reagent) was purchased from Takara Clontech Laboratories (Mountain View, CA, USA). MiR-23a mimic and inhibitor were purchased from Guangzhou Ribobio Co., LTD (Guangzhou, China). The GSK3β inhibitor LY2090314 was obtained from Med Chem Express (NJ, USA). Primary antibodies were obtained from AB clonal technology (Woburn, Massachusetts, USA). Horseradish peroxidase (HRP) and FITC conjugated secondary antibodies were purchased from Cell Signaling Technology (Danvers, MA, USA). Dual luciferase expression vectors (pmirGLO) and dual luciferase reporter assay system was obtained from Promega (Madison, Wisconsin, USA). All other reagents and solvents used were of analytical grade.

2.2. Preparation and characterization of liposomal formulations

2.2.1. Preparation of L-BBR and ML-BBR

Liposomes at a different molar ratio of DSPC, Cholesterol, and Mannose were prepared for bare liposomes (60: 40:0) and Man-bare-liposomes (60:35:5) as described earlier [37]. In brief, each of the components was sequentially added and solubilized in chloroform, which was further mixed with BBR at a ratio of 10:1 in a round bottom flask. A uniform thin film was obtained using a vacuum rotary evaporator (Superfit R150, Mumbai, India) at 40 °C. The deposited thin lipid films were hydrated with PBS (pH 7.4) and were further subjected to water bath sonication and sequential extrusion (at least 11 ×) through a Mini-Extruder (Avanti Polar Lipids, Alabama, USA). F-DHPE incorporated liposomes were prepared at a molar ratio of 60:27.5:7.5:5 was used to perform confocal microscopy. All liposomal formulations were stored at 4 °C for further investigations.

2.2.2. Morphology of liposomal formulations

Surface morphology of formulated liposomes was examined using scanning electron microscopy (SEM), ZEISS EVO 18 Research (Germany) and transmission electron microscopy (TEM), FEI Company, Eindhoven (The Netherlands) as per the previously described procedure [38,39]. Samples were diluted with 0.1 M non-saline phosphate buffer and 11% (w/w) ammonium molybdate solution placed on a 300 mesh copper grid coated with Formvar was used for SEM analysis. For TEM analysis, 5 μl of sample was placed on a 3 mm glow-discharged holey 200 mesh carbon grid with an operating voltage of 120KV was used.

2.2.3. In vitro drug release study

In order to assess the sustained release of berberine from the formulated liposomes, time-dependent (day 1–7) in vitro release was investigated using the dialysis method as published in earlier studies [37,39]. Initially, 1 ml of L-BBR/ML-BBR and free BBR solution was added to activated dialysis membrane (Millipore, 18.2 MΩ cm, USA) and further, suspended in 50 ml of PBS (pH 7.4) release medium at 37 °C stirred at 100 rpm. Samples were withdrawn at pre-set time points from the release medium and analyzed at λ max of 270 nm using a UV–vis spectrophotometer while, simultaneously replacing with fresh release medium each time.

2.2.4. HPLC and FTIR analysis

The encapsulation efficiency of L-BBR/ML-BBR was measured using HPLC as described earlier with few modifications [39]. The mobile phase was a mixture of deionized water and acetonitrile (60:40) at a flow rate of 1.0 ml/min maintained at 30 °C monitored at 270 nm. The drug encapsulation efficiency was calculated as:

$$\%\text{Drug entrapment} = (\text{Total amount of drug} - \text{Free drug})/\text{Total amount of drug} \times 100$$

In order to determine the signature molecules, liposomal formulations mixed with KBr (1:100) was measured from 500 to 4000 cm^{-1} using Fourier-transform infrared spectroscopy (FTIR) analyzer (Shimadzu, Japan).

2.2.5. Particle size and zeta potential

The mean particle size and zeta potential of formulated liposomes were analyzed using dynamic light scattering (DLS) analyzer equipped with zeta potential measuring capacity (Horiba scientific, Japan). In order to investigate the stability of the formulations, liposomes stored at 4 °C and 25 °C for 4 weeks were analyzed at different time periods (days 1, 14 and 30) based on their size, homogeneity, and charge.

2.3. Animals

Wistar albino rats of either sex (120–150 g) were procured from Animal House, Vellore Institute of Technology (VIT), Vellore, India. The animals were cared for in accordance with the guidelines recommended by the Committee for the Purpose of Control and Supervision of Experiments on Animals (CPCSEA), Government of India. All experimental procedures were carried out in compliance with the Institutional Animal Ethical Committee (IAEC), VIT, Vellore, India.

2.4. Isolation and culture of bone marrow-derived monocyte/macrophage

Wistar albino rats of 6–8 weeks were used for the isolation of bone marrow-derived monocytes/macrophage cells as described previously [40]. In brief, the femur bones of the experimental rats were surgically removed and bone marrow was taken out by rapidly flushing with DMEM medium using a 5 ml syringe. For separating the red blood cells, red blood cell lysis buffer was added for 30 s at 37 °C following centrifugation at 1000 rpm for 5 min. Following this, the acquired pellet was washed with ice-cold PBS solution and resuspended in complete DMEM for 12 h. Next, non-adherent cells were removed and the adherent cells were cultured in the presence of 25 ng/ml macrophage-colony stimulating factor (M-CSF) for 3 days under similar culture conditions (Fig. 2). A homogenous population of these monocyte/macrophage-like osteoclast precursor cells between passages 4 to 7 was used for all experiments.

2.5. Cellular uptake study

BMMs isolated were seeded on gelatin-coated round glass coverslips at a density of 1×10^5. Later, osteoclast differentiation was induced by RANKL (100 ng/ml) stimulation and the cells were treated with F-DHPE tagged L-BBR/ML-BBR (12.5 μM) at different time points (12, 24 and 48 h). Post-treatment, cells were fixed with 4% paraformaldehyde and 0.01% glutaraldehyde in PBS incubated overnight at 4 °C. The cells were then mounted in 1, 4-diazabicyclo [2.2.2] octane (DABCO), glycerol and PBS. The cellular uptake was finally examined using a confocal spectral microscope imaging system (Carl Zeiss Microscopy GMBH, Germany) with excitation and emission wavelengths of 496 and 519 nm respectively.

2.6. Cell viability assay

The effect of BBR loaded liposomal formulations on the cellular viability of BMMs was determined using MTT assay as previously illustrated [41]. Briefly, BMMs were initially stimulated with/without RANKL (100 ng/ml) and was further treated with L-BBR/ML-BBR formulations at different concentrations ranging from 0 to 25 μM for another 24 h. Post-treatment, 20 μl of MTT (5 mg/ml in PBS) was added to each well and incubated for 4 h (5% CO_2 at 37 °C) and subsequently, 100 μl of the solubilizing agent (DMSO) was added to get a homogeneous solution for 10 min. Upon color development, plates were analyzed at 570 nm using a microplate reader. The experiments were performed in triplicates.

2.7. Transfection of miR-23a mimic and inhibitor

Transfection of BMMs was performed using X-fect™ RNA transfection reagent following the manufacturer's protocol. BMMs were plated at a density of 1.5×10^6 cells/well in a 6-well culture plate followed by stimulation with RANKL(100 ng/ml) before transfection. Next, 880 μl of serum-free media and 120 μl of transfection cocktail were added to make up the final volume as previously described [42]. miR-23a mimic (50 pMol) was used for enhancing the expression of miRNA alongside a miR-23a inhibitor (50 pMol) as a negative control. After incubation for 4 h, the serum-free media was discarded and DMEM complete medium was added to the cells and incubated for 48 h.

2.8. Dual luciferase reporter assay

Oligos designed for wild type (WT) and mutated GSK3β 3′-UTR

region were individually amplified and cloned into pmiRGLO luciferase reporter plasmid obtained from Promega (Madison, Wisconsin, USA). The primer sequences for the construction of each reporter plasmids used were as follows: Wild-type 3′-UTR of GSK3β (sense: 5′- AAACTA GCGGCCGCAGAGAAGACATCATAGCTAAGTAATGTGAACTGTTAGCCA GCCTAT-3; antisense: 5′CTAGATAGGCTGGCTAACAGTTCACATTACTT AGCTATGATGTCTTCTCTGCGGCCGCTAGTTT-3′) and mutant 3′-UTR of GSK3β (sense: 5′- AAACTAGCGGCCGCAGAGAAGACATCATAGCTA AACTGTTAGCCAGCCTAT3′; antisense: 5′-CTAGATAGGCTGGCTAACA GTTTAGCTATGATGTCTTCTCTGCGGCCGCTAGTTT-3′). Point mutations were induced on the miR-23a binding site using 3′-base substitution of the target sequence [43].

Further, in order to test the potential regulatory activity of miR-23a, GSK3β 3′UTR (WT and mutant) containing pmirGLO vector were co-transfected into BMMs stimulated with RANKL (100 ng/ml) using X-fect™ transfection reagent along with non-specific control and miR-23a mimic. Luciferase assay was performed after 48 h of transfection using dual luciferase reporter assay kit (Promega, Wisconsin, USA). For every sample, the assays were repeated at least three times, and the data for firefly luciferase activity was normalized to that of Renilla luciferase activity as relative fluorescence intensity.

2.9. Quantitative RT PCR analysis

Total RNA was extracted using TRIzol reagent (Sigma Chemicals co., St. Louis, MO, USA) and was reverse transcribed using high capacity cDNA reverse transcription kit (Applied Biosystems, CA, USA) according to the manufacturer's protocol. Gene-specific primers were manually designed using online NCBI primer-BLAST tool and purchased from Sigma Aldrich (St. Louis, MO, USA) [Table 1]. The gene expression was amplified using EvaGreen PCR mastermix (G-Biosciences, St. Louis, MO, USA) following the manufacturer's instructions. The fold change in the expression levels of target genes was relatively quantified after normalization with β-actin values using 2-ΔΔCt comparative cycle threshold method.

2.10. Protein isolation and western blot analysis

Whole-cell lysates were obtained by homogenization in cell lysis RIPA buffer containing protease inhibitor cocktail followed by centrifugation at 14,000 rpm for 15 min at 4 °C. The protein concentration was determined using Bradford's method. 30 μg of protein was separated on 12% SDS-PAGE and electro-transferred onto PVDF membrane (Amersham Pharmacia Biotech, Uppsala, Sweden). The membranes were then blocked with 5% (w/v) BSA overnight at 4 °C and subsequently incubated with rabbit polyclonal primary antibodies against GSK3β, p- GSK3β, NLK1, TAK1, Cathepsin K, CaN and NFATc1 under similar conditions. Later, the blots were washed and then probed for 2 h with horseradish peroxidase (HRP) conjugated secondary antibody. Protein bands were visualized using an enhanced chemiluminescence detection system (Bio-Rad Laboratories, Mississauga, Canada). The blots were stripped and reprobed with β-actin for normalization of protein expression. Each protein blot is representative of three similar independent experiments.

2.11. Immunofluorescence analysis

Immunofluorescence analysis was performed as described previously [42]. Briefly, BMMs were stimulated with/without RANKL (100 ng/ml) followed by treatment with BBR (75 μM), L/ML-BBR (12.5 μM), miR-23a mimic/inhibitor (50 pmol) and LY2090314 (3 μM) for 24 h. Post-treatment, cells were fixed with 4% paraformaldehyde in PBS for 15 min at 37 °C. Thereafter, the cells were washed with 1× PBS and subjected to permeabilization with 0.1% Triton X–100 for 5 min. They were then stained with primary antibody to NFATc1 (1:300) overnight at 4 °C. Further, the cells were incubated with Alexa Fluor 488 conjugated secondary antibody to analyze the expression of NFATc1. The nuclei were counterstained with DAPI for 5 min at 37 °C and imaged using an Olympus fluorescence microscope (Olympus America, Melville, NY, USA). Finally, the mean fluorescence intensity was quantified using Image J software.

2.12. TRAP staining and osteoassay

Briefly, BMMs were seeded in cell culture plates and stimulated with/without RANKL (100 ng/ml). The cells were further transfected with miR-23a mimic/inhibitor and treated with L-BBR/ML-BBR at the indicated concentrations.

In order to ascertain the inhibitory effect of miR-23a and BBR encapsulated liposomal formulations on osteoclast differentiation, TRAP staining was performed according to the manufacturer's protocol (Sigma Aldrich, MO, USA). Multinucleated TRAP-positive osteoclast cells were counted under an inverted microscope for all groups in three independent experiments. Further, to confirm the inhibitory effect on the resorption activity of osteoclasts, BMM cells were seeded in Corning Osteo-Assay 24-well plate (Corning Life Sciences, MA, USA) and cultured as described above. After an incubation period of 5 days, cells were removed using 100 μl of 10% bleach solution for 5 min at room temperature. Later, wells were washed in 1× PBS and air dried for 20 min. The resorption pits formed by activated osteoclast were evaluated and imaged using an inverted microscope (Olympus, Tokyo, Japan) at 40× magnification.

2.13. Gelatin zymography

Gelatin zymography was performed to detect the enzymatic activity of MMP9 as per manufacturer's protocol (Abcam, Cambridge, MA, USA). Briefly, 10 μg of protein containing DMEM medium was run on a 7.5% acrylamide gel at 4 °C with a constant current at 150 V. After washing and overnight incubation, the gels were stained with Coomassie brilliant blue and were further subjected to destaining until clear white bands appeared against a blue background followed by fixing in preservation buffer for further imaging.

2.14. Statistical analysis

The data were presented as mean ± standard error mean (SEM). Statistical analysis was performed using one-way analysis of variance (ANOVA) with Bonferroni's post-test using graph pad 5.0 for windows.

Table 1
Primer sequences used for quantitative real-time PCR analysis.

Gene	Forward	Reverse
MMP9	5′-GAAAACCTCCAACCTCACGG-3′	5′-CTCTAGACATGCCCATCACTCC-3′
Cathepsin K	5′-AAGGATATTGTGAGCTGGGGAC-3′	5′-CCGCTCTTGAGAAAGGCTTACA-3′
TRAP	5′-CTCTTCTACTGAGAGGTGCGA-3′	5′-CAGCACCATCCACGTATCCA-3′
CaN	5′-ACAATCGGCGTGGGGAAG-3′	5′-GCACACGGTCGGTCGGATTAAGA-3′
TAK1	5′-GAGTATGGTGGTCTGAGAAAAGC-3′	5′-AGTGGAGTTTGGCTTAGGTTG-3′
NFATc1	5′-CACACTGTGAAGGGTGTCCC-3′	5′-CCATCCTCAAATCTCACCCGT-3′
β-actin	5′- ACCACCATGTACCCAGGCATT-3′	5′-CACACAGAGTACTTGCGCTCA-3′

Values depicting $^{*\#}P < 0.05$ were considered to be statistically significant.

3. Results

3.1. Synthesis and characterization of formulated liposomes

In order to achieve the sustained release of berberine (BBR), two types of liposomal formulations (L-BBR/ML-BBR) were prepared by the conventional thin film hydration method. Further, successive ultra-sonications and sequential extrusions were performed to obtain the homogeneous single uni-lamellar vesicles (SUVs) (Fig. 1a & b). The particle size and zeta potential of L-BBR was found to be 125.1 nm ± 3.2 and −31.87 mV ± 3.05, and the ML-BBR showed 153.5 nm ± 2.4 nm and −39.0 mV ± 2.3 respectively at 0th day (Table 2). The negative zeta potential value obtained for the prepared liposomal formulations (L-BBR and ML-BBR) depicts their physical stability that prevented their aggregation and promoted the ionic interaction with the surface of BMMs. The stability with regard to particle size and zeta potential after incubation for a week (7th day) and a month (28th day) time period at different storage conditions (4 and 25 °C) showed minor negligible changes (Table 2). Subsequently, the SEM and TEM images illustrated that the liposomal formulations (Bare and ML-liposomes) with/without berberine were homogeneous in size and spherical in shape (Fig. 1c & d).

In order to confirm the entrapment of BBR within the formulated liposomes, Fourier-transform infrared spectroscopy (FTIR) analysis was performed. Fig. 1e & f highlights the FTIR spectra for L-BBR and ML-BBR. For L-BBR, the characteristic absorption peaks at 3306.99 and 1636.64 cm^{-1} were attributed to the cholesterol and BBR structures. Similarly, the peaks at 3282.81, 1637.56 and 1036.77 cm^{-1} for ML-BBR overlapped with the cholesterol, berberine and mannose molecules respectively. Further, the drug entrapment efficiency (EE) of L-BBR/ML-BBR immediately after the preparation elicited a value of 88.5% and 95% as detected by HPLC (Fig. 1g) whereas, it was noted that the EE decreased with further incubation for 30 days. However, a higher EE of ML-BBR (65%) was found as compared to L-BBR (53%) that signifies its better bio-availability. To investigate the sustained and controlled release of BBR from the formulated liposomes, in vitro drug release study was performed over a period of 10 days. The data analyzed using UV spectrophotometer, at 270 nm, revealed a sustained release of L-BBR and ML-BBR as compared to the immediate dissolution of free-BBR (Fig. 1h). Therefore, BBR loaded liposomal formulations were used immediately after appropriate sonication and extrusion for all further experiments. Evidently, a time-dependent (12, 24 and 48 h) uptake study of L-BBR and ML-BBR in BMMs showed that mannosylation of liposome has potentially increased its preferential internalization towards macrophages as compared to unmodified L-BBR (Fig. 1i & j). It was also noticed that internalization of ML-BBR was efficient at the end of the 48 h time period. Based on this, a 48 h treatment was followed for subsequent experiments.

3.2. Effect of BBR encapsulated liposomes on the cell viability of BMMs

To determine the cytotoxic effect of BBR encapsulated liposomes (L-BBR and ML-BBR) on the cell viability of BMMs, MTT assay was performed. BMMs stimulated with RANKL (100 ng/ml) were exposed to varying concentrations of L-BBR and ML-BBR (2.5 to 25 μM) for 24 h. The results showed significant alterations to cellular viability at concentrations above 15 μM (Fig. 2a & b). Maximum cell viability for both liposomal formulations was observed up to 12.5 μM concentration. Therefore, for subsequent experiments 12.5 μM concentrations of L-BBR and ML-BBR were used. For comparative analysis, free-BBR at a concentration of 75 μM was used based on our previously reported study [35].

3.3. ML-BBR up-regulates miR-23a levels in BMMs

The previous study from our lab reported the upregulating effect of BBR (25–75 μM) on the expression of miR-23a in LPS/TNFα stimulated RAW 264.7 and adjuvant-induced arthritic synovial macrophage (AA-SM) cells [35]. Similarly, we analyzed the gene expression levels of miR-23a in BMMs with/without RANKL stimulation. The level of miR-23a was significantly suppressed in RANKL stimulated BMMs (Fig. 5f). Upon treatment with L-BBR/ML- BBR, a significant increase in miR-23a expression was observed. However, ML-BBR exhibited a two-fold increase in miR-23a levels as compared to L-BBR and free BBR treatment. Additionally, p-GSK3β inhibitor (3 μM) treatment also resulted in a basal level expression of miR-23a, thereby supporting the regulatory role of miR-23a in RANKL/p-GSK3β pathway.

3.4. Effect of ML-BBR on gene and protein expression levels

To further unravel the therapeutic efficacy of BBR encapsulated liposomes (L-BBR/ML-BBR) towards osteoclast differentiation and activation, we assessed the mRNA expression levels of NFATc1, MMP9, Cathepsin K, TRAP, CaN and TAK1 in RANKL (100 ng/ml) stimulated BMMs (Fig. 3a–f). The results showed that RANKL stimulation on BMMs dramatically increased the levels of NFATc1, MMP9, Cathepsin K, TRAP and CaN whereas, treatment with free BBR (75 μM), L/ML-BBR (12.5 μM) reduced their expression, with an increased expression of TAK1, a natural inhibitor of GSK3β pathway. MiR-23a mimic (50 pmol) transfection and LY2090314 (3 μM) also exhibited a similar expression pattern to ML-BBR treated group. To further strengthen our findings from the gene profiling studies, the protein expression of GSK3β/p-GSK3β, NFATc1, NLK1, TAK1 and CaN in RANKL (100 ng/ml) stimulated BMMs was performed (Fig. 4a-g). Moreover, the activation of NFATc1 was analyzed using immunofluorescence assay (Fig. 4h & i). The results showed that upon RANKL stimulation the levels of p-GSK3β, NFATc1 and CaN were elevated. Contrastingly, natural inhibitors of GSK3β pathway namely, NLK1 and TAK1 kinases were found to be significantly inhibited. Post-treatment with free-BBR, L/ML-BBR a sharp decrease in p-GSK3β, NFATc1, and CaN expression was observed. Additionally, miR-23a mimic and LY2090314 treatment also suppressed the levels of these factors depicting that miR-23a has direct control over GSK3β/p-GSK3β and its mediated effector molecules involved in osteoclastogenesis and bone erosion.

3.5. ML-BBR treatment downregulated MMP9 levels

MMP9 belongs to a family of zinc-dependent endopeptidases involved in ECM degradation which results in bone erosion and abnormality in arthritis. The enzymatic activity of MMP9 was estimated using gelatin zymography as demonstrated in Fig. 3g. While MMP9 levels were found to be increased in RANKL stimulated group, ML-BBR treatment inhibited the MMP9 expression better than L-BBR and frees BBR. In p-GSK3β inhibitor (LY-2090314) and miR-23a mimic treated groups, the MMP9 expression was found to be significantly suppressed indicating that ML-BBR treatment inhibited RANKL/p-GSK3β mediated osteoclast activity via possible regulation of miR-23a.

3.6. ML-BBR treatment inhibited the osteoclastogenic potential of RANKL stimulated BMMs

To investigate the inhibitory potential of ML-BBR on RANKL mediated osteoclast differentiation, TRAP staining, and pit formation assay were performed. It was observed that there was a significant increase in the number of TRAP-positive osteoclast cells in RANKL stimulated group whereas, ML-BBR treatment exhibited significant inhibition of osteoclast cells in comparison to L-BBR and free BBR treated groups (Fig. 5a & b). Subsequently, miR-23a mimic transfected and LY2090314 (3 μM) treated group also inhibited the differentiation of

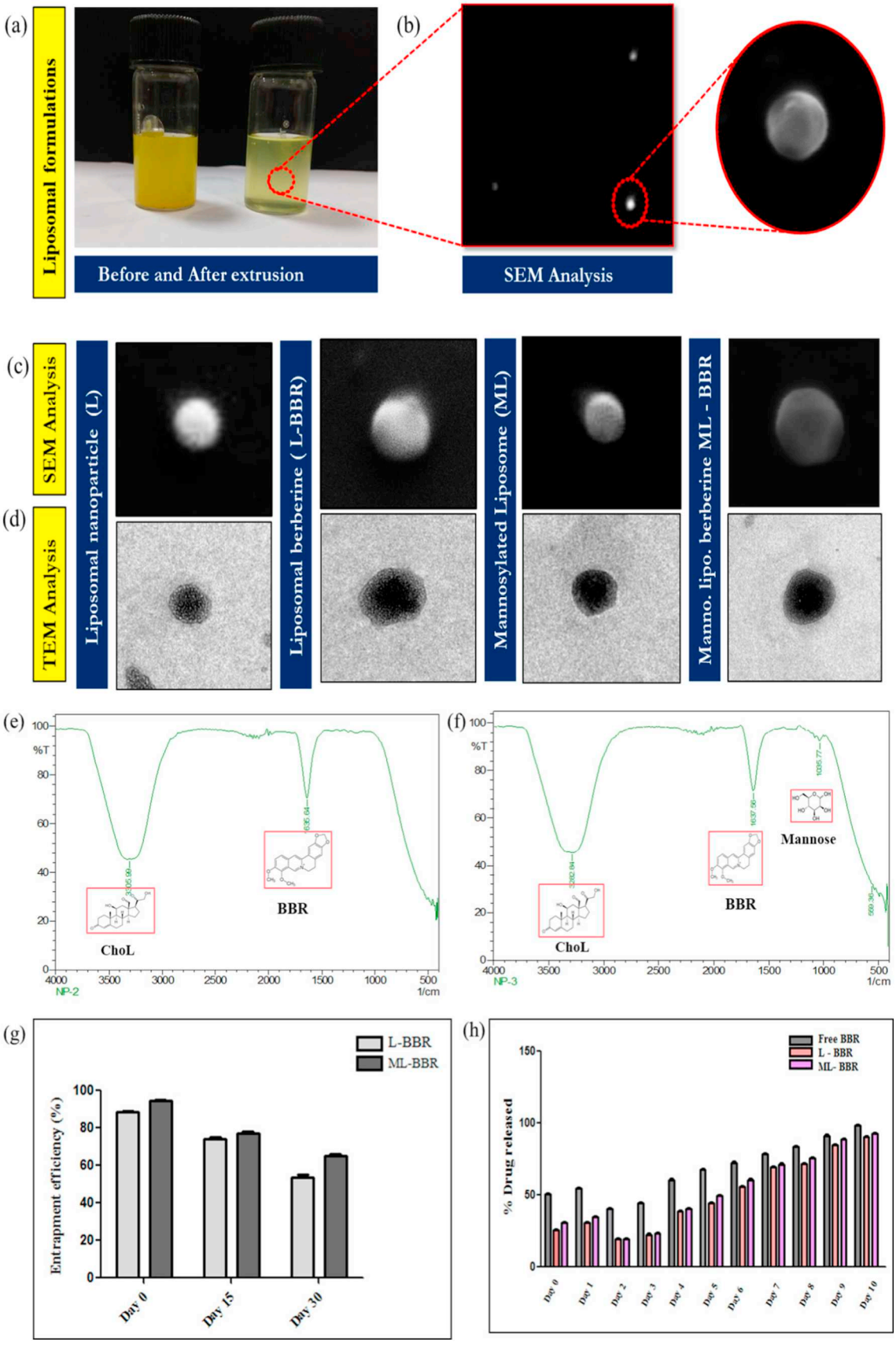

(caption on next page)

Fig. 1. (a) The liposomal samples encapsulated with berberine before and after extrusion. (b) The scanning electron microscopy (SEM) images of the prepared liposomes with spherical morphology. (c) SEM and (d) TEM images of L-BBR and ML-BBR. Scale bars ~ 200 nm. FTIR spectroscopic analysis of (e) L-BBR and (f) ML-BBR were measured between 500 and 4000 cm^{-1}. (g) The percentage of BBR entrapped within the liposomal formulated vesicle over different time points (0–30 days) was determined using HPLC analysis. (h) In vitro drug release study was performed using dialysis method at different time intervals (Day 1 to 10). Confocal microscopic images of (i) L-BBR (12.5 μM) and (j) ML-BBR (12.5 μM) on RANKL (100 ng/ml) stimulated BMMs at different time intervals (12, 24 and 48 h) signifies the affinity and internalization of formulated liposomes. Scale bars ~ 10 μm.

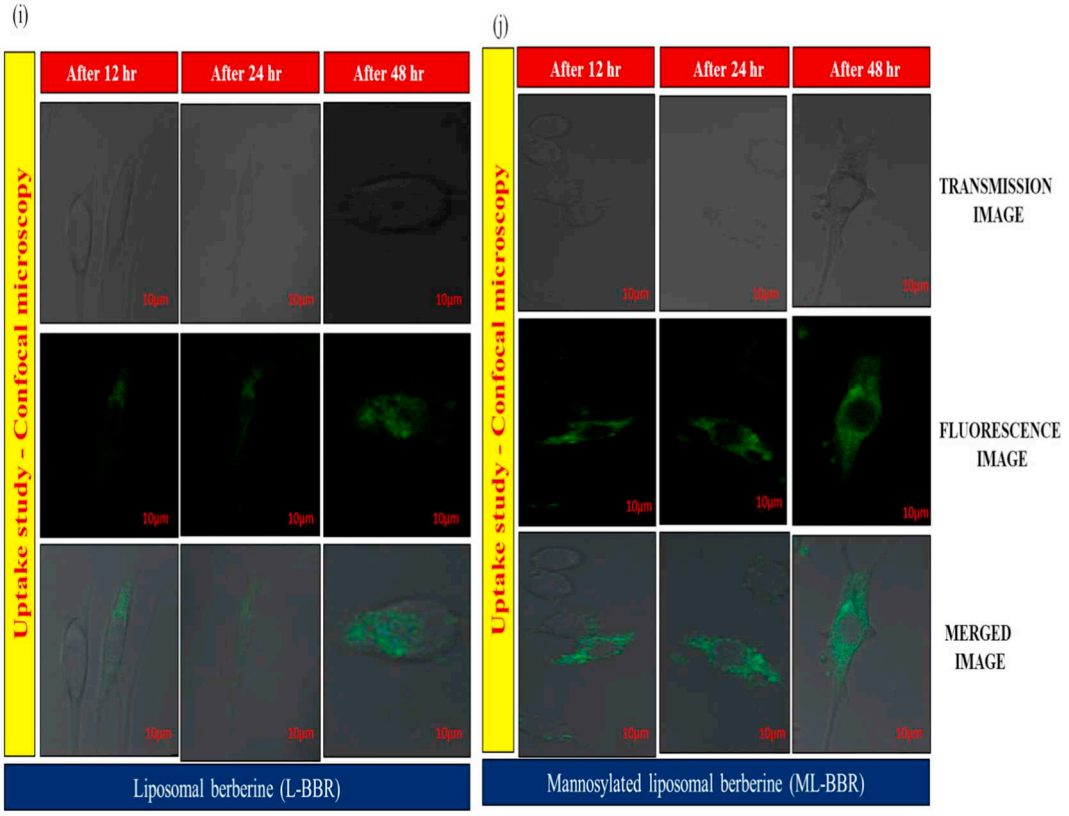

Fig. 1. (*continued*)

osteoclast precursor cells.

We further explored the anti-osteoclastic potential of ML-BBR using osteoclastic bone resorption assay. BMMs stimulated with RANKL (100 ng/ml) on the bone mimetic synthetic surface plates showed significantly large and more number of resorption pits when compared with an unstimulated group (Fig. 5c & d). Treatment with free BBR, L/ML-BBR markedly decreased the osteoclast promoting the potential of RANKL stimulated BMMs as evidenced by the smaller and reduced number of resorption pits, whereas, treatment with ML-BBR exhibited a better inhibition of resorption pits. Evidently, miR-23a mimic transfected and LY2090314 (3 μM) treated group also reduced the number of resorption pits. Taken together, it can be seen that RANKL/p-GSK3β mediated osteoclastogenic activity was downregulated by ML-BBR through the induction of miR-23a.

3.7. Direct targeting of GSK3β by miR-23a

In order to confirm the regulatory effect of miR-23a on the activity of GSK3β, initially, we performed target Scan that reported GSK3β mRNA to be one of the potential targets of miR-23a (Fig. 5e). It was

Table 2
Particle size and zeta potential of L-BBR and ML-BBR at different temperature and time intervals were analyzed using DLS instrument. Data are represented as mean ± SEM.

L-BBR					ML-BBR				
Particle size (nm)			Zeta potential (mV)		Particle size (nm)			Zeta potential (mV)	
Temperature	Day 0	Day 7	Day 0	Day 7	Temperature	Day 0	Day 7	Day 0	Day 7
4 °C	127.4 ± 2.4	131.6 ± 3.6	−33.6 ± 2.8	−31.2 ± 3.6	4 °C	154.6 ± 1.6	156.8 ± 2.4	−33.6 ± 2.8	−31.6 ± 3.8
	126.8 ± 3.2	132.4 ± 1.8	−31.8 ± 4.2	−32.4 ± 2.8		152.86 ± 2.4	158.24 ± 3.2	−31.8 ± 4.2	−32.4 ± 3.2
25 °C	123.4 ± 4.6	134.2 ± 3.2	−30.26 ± 2.8	−28.6 ± 3.6	25 °C	153.84 ± 3.0	154.8 ± 2.6	−29.6 ± 2.4	−30.68 ± 1.8
	122.8 ± 2.8	133.8 ± 2.6	−31.84 ± 2.4	−29.8 ± 2.8		152.8 ± 2.6	151.6 ± 2.2	−30.8 ± 1.8	−31.4 ± 2.2
Temperature	Day 14	Day 28	Day 14	Day 28	Temperature	Day 14	Day 28	Day 14	Day 28
4 °C	138.6 ± 2.2	156.46 ± 2.4	−38.2 ± 2.8	−34.2 ± 2.68	4 °C	162.6 ± 1.86	174.4 ± 1.46	−34.68 ± 1.4	−41.6 ± 1.84
	142.42 ± 1.48	154.86 ± 2.16	−34.4 ± 4.2	−33.46 ± 1.84		166.16 ± 1.46	178.24 ± 2.4	−33.18 ± 3.16	−42.4 ± 2.26
25 °C	148.4 ± 2.4	158.42 ± 3.2	−32.46 ± 2.16	−30.6 ± 2.81	25 °C	170.44 ± 2.4	184.48 ± 1.8	−39.6 ± 1.84	−40.68 ± 2.86
	152.6 ± 3.16	154.48 ± 1.68	−33.54 ± 2.6	−32.8 ± 1.86		172.8 ± 2.6	181.36 ± 1.96	−36.84 ± 2.16	−41.46 ± 3.24

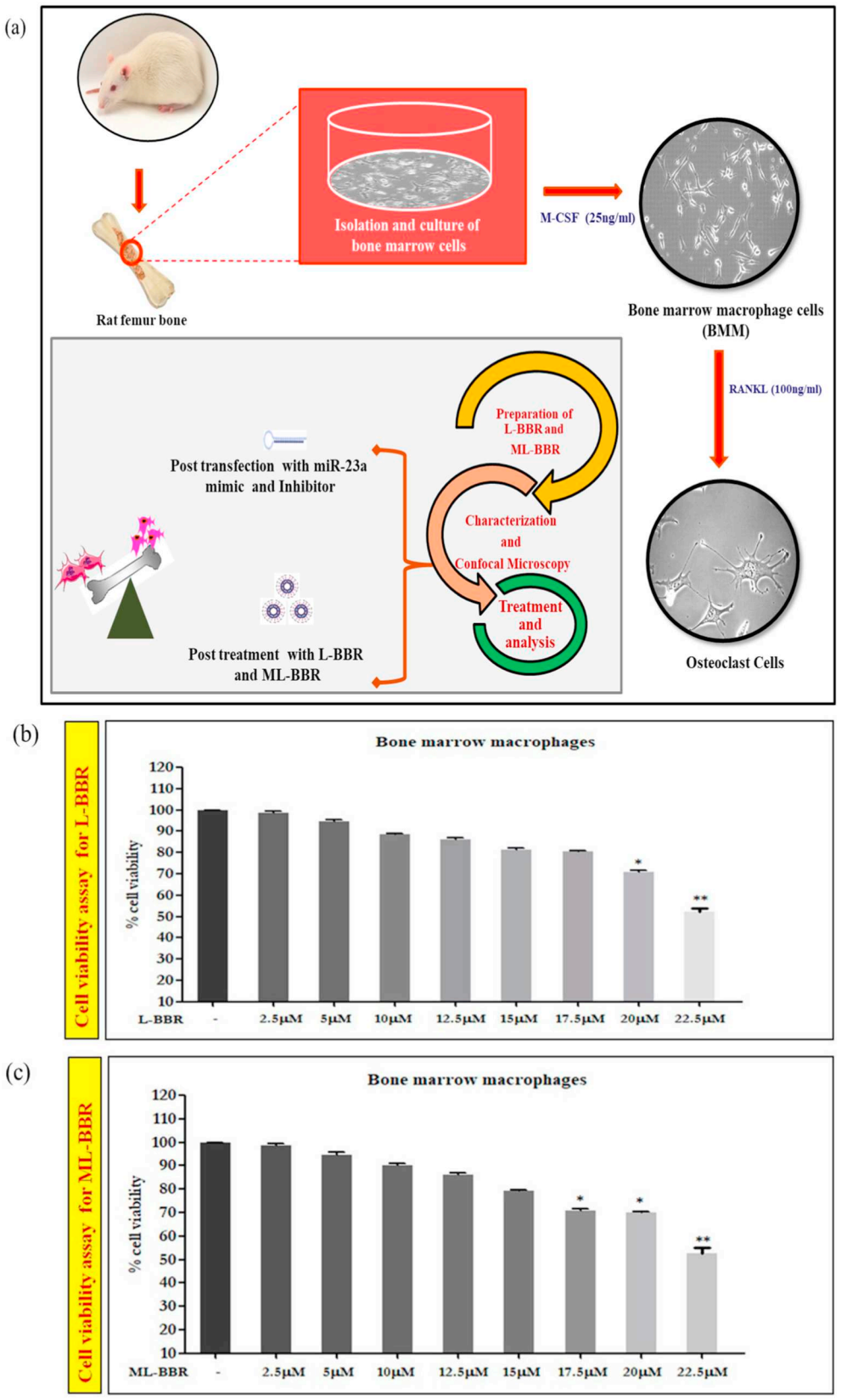

Fig. 2. (a) Schematic representation for the isolation, culture, and treatment of Bone marrow-derived monocytes/macrophages (BMMs). Effect of (b) L-BBR and (c) ML-BBR on the cellular viability of RANKL (100 ng/ml) stimulated BMMs. Cells were seeded in a 96-well plate and treated for 24 h with different concentrations of drug-loaded liposomes. Cell viability was measured using MTT assay. Experiments were performed in triplicates. Data are presented as mean ± SEM. $^{*}P < 0.05$ compared with untreated control group.

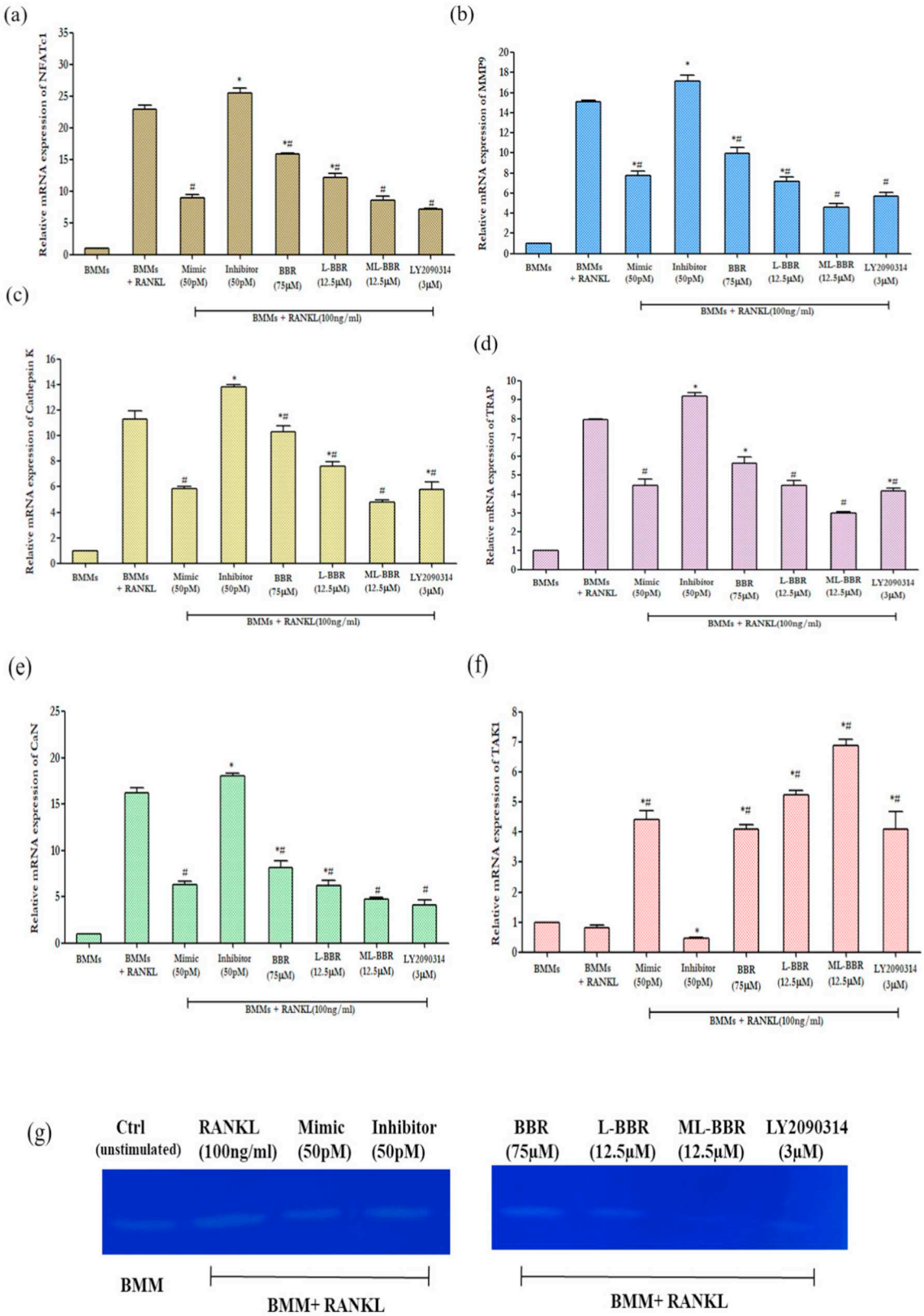

Fig. 3. Effect of ML-BBR (12.5 μM) on gene expression levels of NFATc1, MMP9, cathepsin K, TRAP, CaN and TAK1. (a–f) Relative gene expression of NFATc1, TAK1, cathepsin K, TRAP, CaN and MMP9. (g) Gelatin zymography of MMP9. Comparisons are made with: *BMMs versus miR-23a mimic/inhibitor (50 pmol) and BBR (75 μM)/L-BBR (12.5 μM)/ML-BBR (12.5 μM)/LY2090314 (3 μM); #BMMs + RANKL (100 ng/ml) versus miR-23a mimic/inhibitor (50 pmol) and BBR (75 μM)/L-BBR (12.5 μM)/ML-BBR (12.5 μM)/LY2090314 (3 μM). *#$P < 0.05$ implies statistically significant.

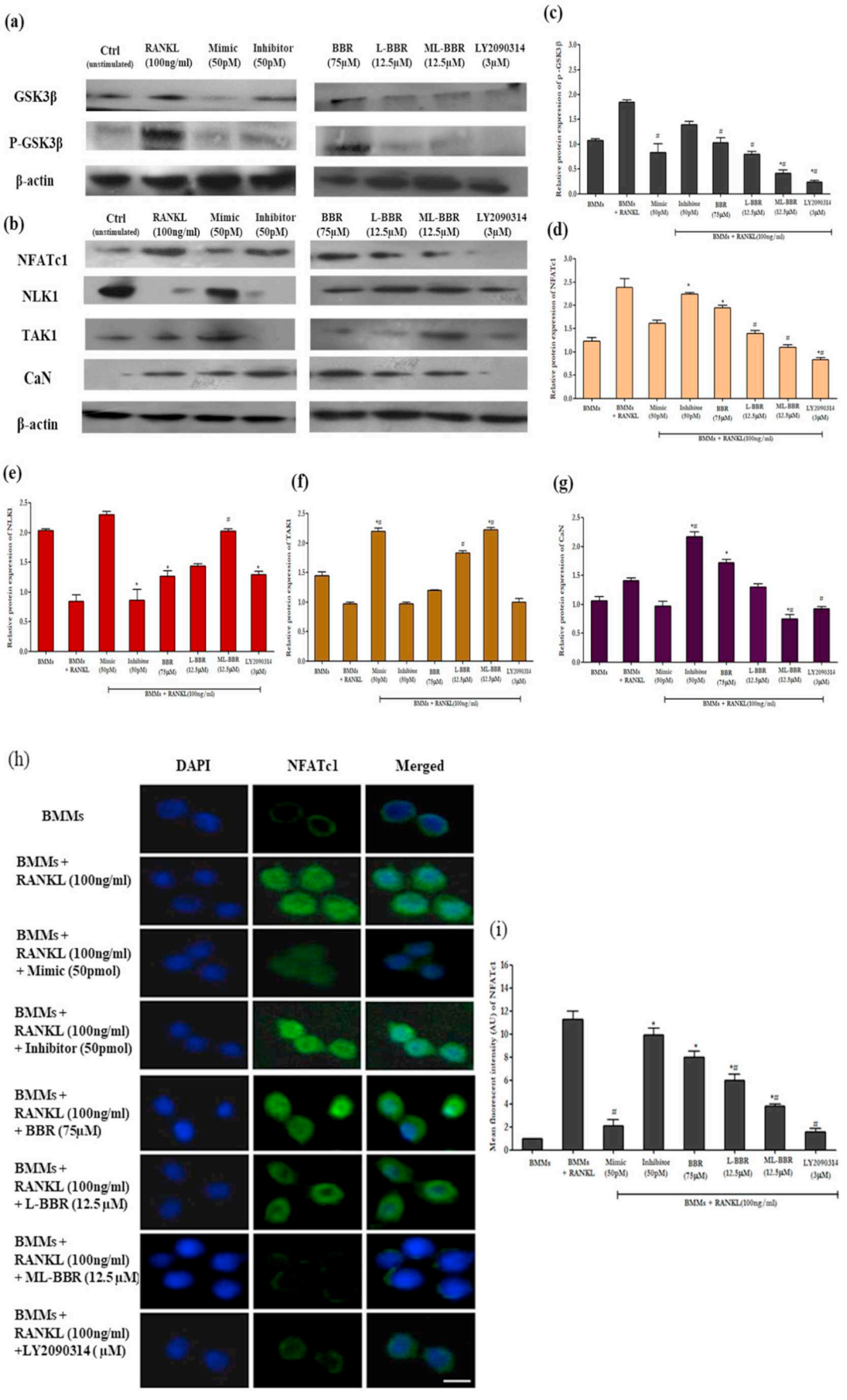

(caption on next page)

Fig. 4. Effect of ML-BBR (12.5 μM) on protein expression levels of GSK3β/p-GSK3β, NLK1, TAK1, NFATc1 and CaN in BMMs. (a & b) Western blot images of GSK3β/p-GSK3β, NLK1, TAK1, NFATc1 and CaN. (c–g) Relative protein expression of GSK3β/p-GSK3β, NLK1, TAK1, NFATc1 and CaN. Effect of ML-BBR (12.5 μM) on the expression levels of NFATc1 protein in RANKL (100 ng/ml) stimulated BMM cells was determined by immunofluorescence analysis (h & i). Comparisons are made with: *BMMs versus miR-23a mimic/inhibitor (50 pmol) and BBR (75 μM)/L-BBR (12.5 μM)/ML-BBR (12.5 μM)/LY2090314 (3 μM); #BMMs + RANKL (100 ng/ml) versus miR-23a mimic/inhibitor (50 pmol) and BBR (75 μM)/L-BBR (12.5 μM)/ML-BBR (12.5 μM)/LY2090314 (3 μM). *#P < 0.05 implies statistically significant. Scale bars ~10 μm.

further validated using western blot analysis that showed transient transfection of miR-23a was able to inhibit GSK3β/p-GSk3β activity (Fig. 4a and c). To further strengthen this theory, we performed dual luciferase reporter assay. The pmiRGLO construct (Promega, Wisconsin, USA) containing firefly luciferase and Renilla luciferase was used for the cloning of GSK3β 3′ UTR. The firefly luciferase activity in the vector system was constitutively expressed and used for normalization with that of Renilla luciferase activity. The pmiRGLO construct was transiently co-transfected with control miRNA or miR-23a mimic (50 pmol) in BMMs. After 48 h of treatment, there was a significant decrease in the luciferase activity when BMMs were transfected with the pmiRGLO containing WT- GSK3β 3′ UTR along with miR-23a mimic (Fig. 5g). The mutant GSK3β 3′ UTR was not significantly affected after transfection with the control miRNA and mimic miR-23a, depicting the modulatory role of miR-23a on GSK3β expression.

4. Discussion

In recent years, it is evident that epigenetic regulators such as microRNAs (miRNAs) control several aspects of bone loss associated with bone-related deformities. Numerous studies have also recently explored the importance of miRNAs as potential biomarkers for the prognosis and treatment of bone disorders [44]. The cluster spanning from miR-17-92 predominantly have been explored to play a key role in controlling the enhanced functional activity of osteoclast cells that performs the bone resorption part of bone remodeling [45]. Notably, miR-23a has been designated to be a key component possessing the potential to control various inflammatory processes which incidentally have the least reports explaining its efficiency [46]. It belongs to the miR-23 gene family consisting of hsa-miR-23a and hsa-miR-23b [47]. So far, several reports have implicated the role of miR-23a in preventing the occurrence of cancer as well as arrest its progression [48,49]. Additionally, a recent report has suggested the role of miR-23a and miR-23b in balancing osteoblast and adipocyte differentiation in bone marrow mesenchymal stem cells (BMSCs). Further, this elicited that the downregulation of miR23a/b in age-related osteoporosis reduced the capacity of BMSCs to differentiate into osteoblasts instead of adipocytes [50]. Moreover, a recent study has demonstrated the physiological functions of miR-23a cluster, which consists of miR-23a, miR-27a, and miR-24-2 on the osteoblast lineage in transgenic gain-of-function (GOF) and loss-of-function (LOF) mouse model [51]. Also, more attention has been devoted to study the role of miR-23a in the impaired differentiation of osteoblast cells during osteosarcoma [52]. In conjunction with these reports, our study investigated the immunomodulatory role of miR-23a on the expression of p-GSK3β mediated NFATc1 signaling in osteoclast-mediated bone erosion.

Although exclusively studied, many mechanisms controlling joint inflammation and osteoclastogenesis resulting in bone erosion are poorly understood. Several signaling pathways like nuclear factor kappa B (NF-κB), mitogen-activated protein kinases (MAPKs) (ERK, JNK, p38) and Wnt signaling are considered to be activated downstream of RANKL. Moreover, monocytes/macrophages in response to RANKL activate a major transcription factor, NFATc1, which promotes the differentiation and regulation of osteoclast cells [53,54]. Osteoblast-lineage cells and osteoclast precursors predominantly express RANKL, whereas noncanonical Wnt signaling via p-GSK3β in osteoclast precursors enhanced RANKL-induced osteoclastogenesis [55,56]. Thus, it is likely that this pathway helps to ensure proper skeletal homeostasis during bone remodeling. As bone resorption is a major phenomenon of various inflammatory disorders of the joints, we unraveled the role of RANKL/p-GSK3β signaling in BMMs during pathophysiological conditions [57]. Notably, studies have demonstrated that RANKL stimulation increases the phosphorylation of GSK3β thereby inducing the nuclear translocation of NFATc1 [13]. Given that NFATc1 is a key regulator of osteoclast activation, its activity has been shown to be upregulated by activated calcineurin (CaN), a diphosphatase, that further regulates the transcription of osteoclastogenic genes like TRAP, cathepsin K and MMP-9 via exposing the nuclear localization signal of NFATc1 [58]. Hence, our results have also shown that stimulation of BMMs with RANKL significantly increased the expression of both p-GSK3β and CaN, which would suggest that phosphorylation of GSK3β might activate NFATc1 in conjunction with the activation of CaN. Additionally, our outcomes firmly suggest that RANKL mediated p-GSK3β signaling is modulated by miR-23a in RANKL stimulated BMMs. Through dual luciferase reporter assay, we found that miR-23a inhibited the expression of GSK3β. Similarly, miR-23a mimic transfection also remarkably inhibited both GSK3β and p-GSK3β at the protein level. Based on these results, it is suggested that the action of miR-23a in the regulation of p-GSK3β is via complete inhibition of GSK3β at the post-transcriptional level. In addition, the introduction of miR-23a mimic into the system also served as direct control over the secretion of major osteoclast differentiating factors. Thus, these outcomes provide strong evidence for the inhibitory effect of miR-23a on RANKL mediated p-GSK3β signaling in osteoclastogenesis. However, miR-23a transfection showed an increased level of Nemo-like kinase 1 (NLK1) and TGFβ activated tyrosine kinase 1 (TAK1), the negative regulators for GSK3β pathway and down-regulated the expression level of NFATc1 [59]. Thus, miR-23a may be a therapeutic target for the treatment of bone diseases with abnormal bone resorption.

In the present study, we chose BBR, an isoquinoline quarternary alkaloid from plants that have been associated with a broad spectrum of biological activities that includes inhibition of RANKL-mediated osteoclastogenesis. It has also been reported that BBR has the potential for inhibiting the p-GSK3β levels in diabetic rat models [26]. A previous study from our lab has reported the upregulating effect of BBR on the expression of miR-23a in LPS/TNFα stimulated RAW 264.7 and adjuvant-induced arthritic synovial macrophage (AA-SM) cells [42]. Similarly, in this study, we have shown that berberine can upregulate the level of miR-23a in RANKL stimulated BMMs. All together we can conclude that berberine is modulating GSK3β via miR-23a for inhibiting osteoclast differentiation. Due to its poor solubility in aqueous buffers and it's short half-life in circulation, it has been reported that encapsulating BBR into circulating liposomes improved its therapeutic availability and efficacy [60]. Since the liposomal drug delivery system is a well-approved drug carrier due to its non-toxic, non- carcinogenic and biodegradable properties, in the present study, we have utilized single unilamellar liposomal nanoparticles. In line with these results, various liposomal formulations encapsulated with BBR (L-BBR and ML-BBR) were prepared by thin film hydration method and characterized. Additionally, mannose ligands on the liposomal formulation were

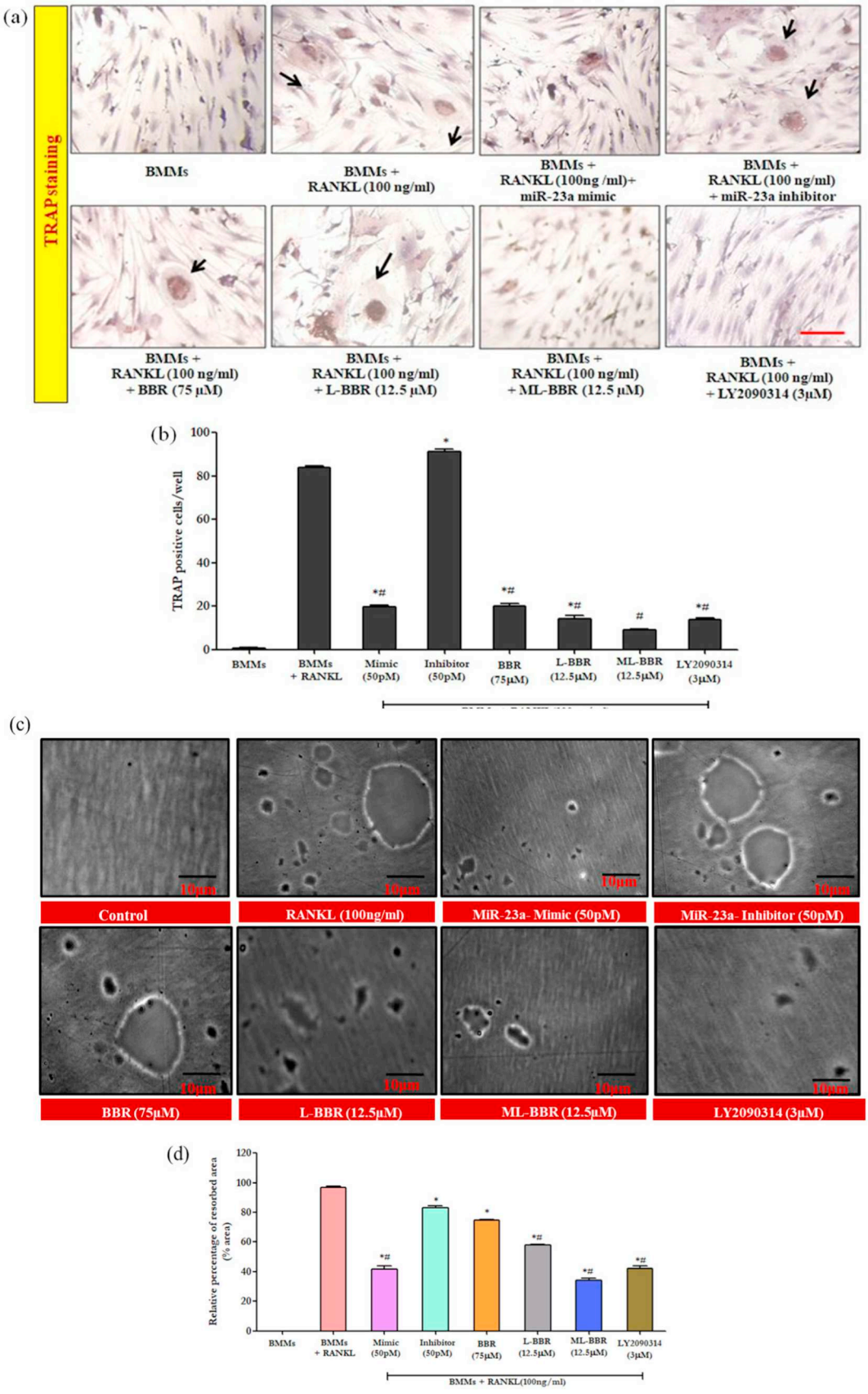

(caption on next page)

Fig. 5. Effect of ML-BBR (12.5 μM) towards osteoclast differentiation. (a) TRAP staining analysis. (b) A total number of relative TRAP-positive cells. Effect of ML-BBR (12.5 μM) on the bone resorptive activity of BMMs. (c) Osteoassay analysis of BMMs stimulated with RANKL (100 ng/ml). (d) Relative resorptive activity of BMMs. miR-23a directly targets GSK3β 3′UTR. (e) Target Scan analysis of GSK3β with miR-23a. (f) Gene expression levels of miR-23a in BMMs. (g) Luciferase analysis of the wild type and mutant GSK3β 3′ UTR. Comparisons are made with: *BMMs versus miR-23a mimic/inhibitor (50 pmol) and BBR (75 μM)/L-BBR (12.5 μM)/ML-BBR (12.5 μM)/LY2090314 (3 μM); #BMMs + RANKL (100 ng/ml) versus miR-23a mimic/inhibitor (50 pmol) and BBR (75 μM)/L-BBR (12.5 μM)/ML-BBR (12.5 μM)/LY2090314 (3 μM). *#P < 0.05 implies statistically significant. Scale bars ~10 μm.

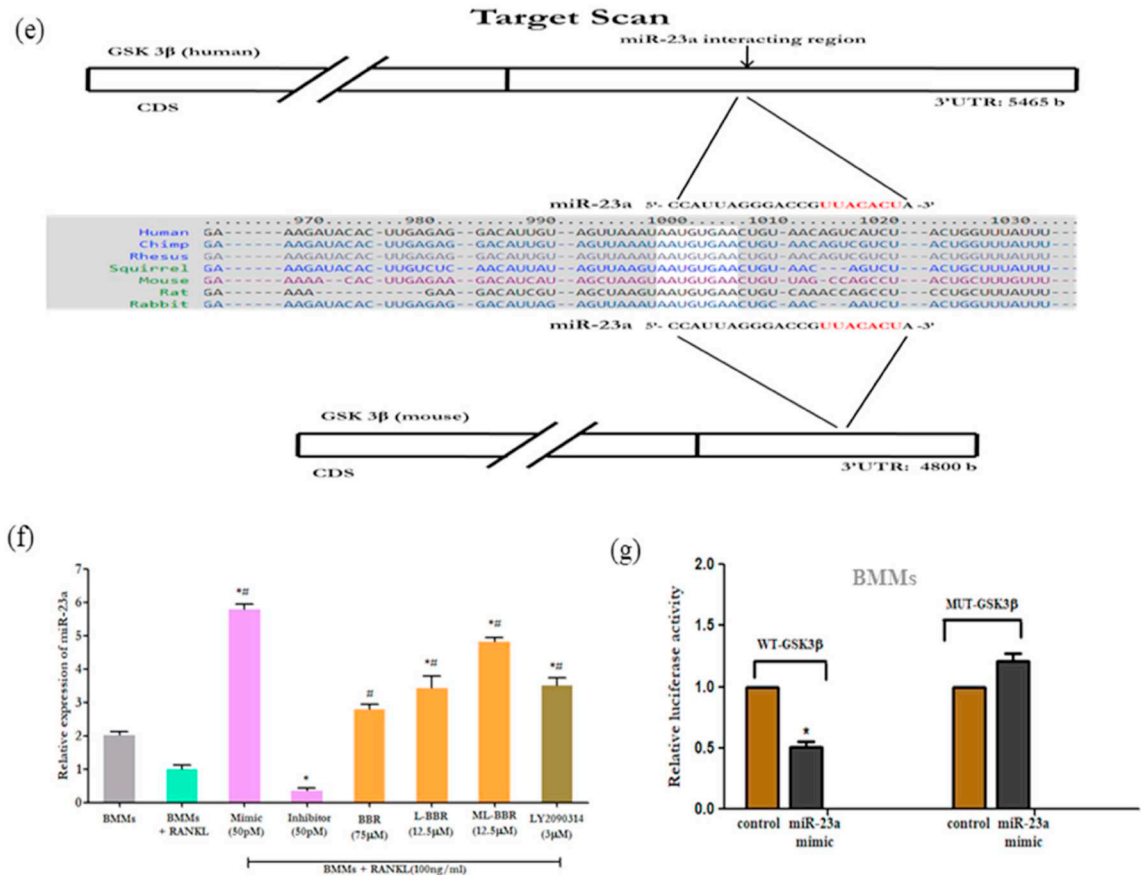

Fig. 5. (*continued*)

shown to preferentially target the activated macrophages due to their potent phagocytic behavior when compared to the normal macrophages during osteoclastogenesis; thereby enhancing their cellular uptake [39]. Additionally, the presence of c-lectin-type receptors on the surface of the macrophages was stimulated by the mannose ligands coated over the liposomes, further increasing their internalization preferentially towards activated macrophages. [61]. Therefore in the current study, we have treated the RANKL stimulated BMMs with berberine encapsulated mannosylated liposomes (ML-BBR) to evaluate their specific inhibitory action on osteoclastogenesis and their anti-resorptive activity. We witnessed a diminished expression level of p-GSK3β; NFATc1 and calcineurin (CaN) through induction of NLK1 and TAK1 in BMMs after ML-BBR treatment as compared to free-BBR treatment. Further experimental studies have revealed that after treating the cells with ML-BBR an upregulation of miR-23a level was recorded which resulted in the deterioration of osteoclastogenesis and bone resorptive activity. Recent reports have strongly suggested the extensive role of MMP9 in promoting the invasive phenotype of osteoclasts through ECM degradation [62]. In support of this notion, our study detected the elevated levels of MMP9 in RANKL stimulated BMMs as compared to its control group. We further witnessed that ML-BBR treatment and miR-23a transfection significantly reduced the expression levels of MMP9, which further potentiates the anti-bone resorptive activity. Hence, the inhibition of these osteoclastogenic factors observed in our present study upon selective inhibition by ML-BBR via upregulation of endogenous miR-23a level strongly provides strong evidence for its potency as a therapeutic intervention in bone-related disorders.

5. Conclusion

Overall, our current study demonstrated that preferential internalization of berberine via mannose coated liposomal delivery system (ML-BBR) attenuated mature osteoclast formation via suppressing RANKL dependent p-GSK3β/NFATc1 signaling through the activation of miR-23a. Berberine is a potent inhibitor of osteoclastogenesis and suppressed GSK3β especially its phosphorylated form. Furthermore, it upregulated the level of miR-23a, a specific inhibitor of GSK3β. Targeted delivery of BBR in the form of ML-BBR potentially inhibited the bone resorption activity of osteoclasts by suppressing the expression of bone resorptive enzymes like TRAP, Cathepsin K and MMP9. Therefore, we concluded that ML-BBR potentially represents a possible therapeutic intervention, which readily ameliorates osteoclast-mediated bone erosion and acts as a therapy for debilitating bone loss disorders (Schematically represented in Fig. 6).

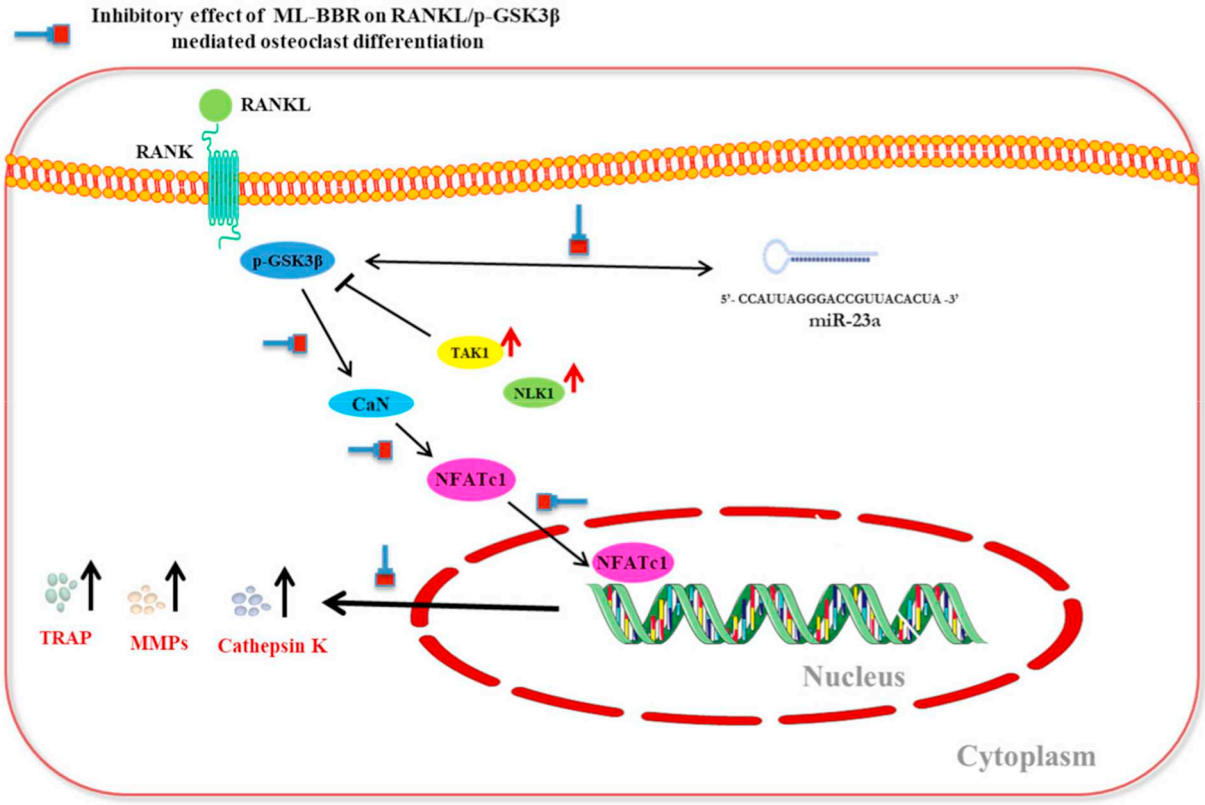

Fig. 6. Overall therapeutic effect of ML-BBR against RANKL mediated p-GSK3β/NFATc1signaling cascade in BMMs. ML-BBR attenuated osteoclastogenesis in RANKL stimulated BMMs through the inhibition of p-GSK3β/CaN/NFATc1 pathway and by inducing the expression of miR-23a. Notes: mannosylated liposomal berberine (ML-BBR); glutathione synthase kinase 3 beta (GSK3β); microRNA 23a (miR-23a); nuclear factor activator of T-cells 1 (NFATc1), Calcineurin (CaN); nemo-like kinase 1 (NLK1); receptor activator of nuclear factor kappa B ligand (RANKL); TGF-β activated kinase 1 (TAK1).

Declaration of Competing Interest

The authors declare that they have no conflict of interest.

Acknowledgment

Sali Sujitha would like to thank University Grants Commission-Maulana Azad National Fellowship (UGC-MANF) for providing financial assistance in the form of Junior Research Fellowship (JRF) [ID no: MANF-2017-18-KER-82149].

References

[1] G. Schett, E. Gravallese, Bone erosion in rheumatoid arthritis: mechanisms, diagnosis and treatment, Nat. Rev. Rheumatol. 8 (2012) 656–664, https://doi.org/10.1038/nrrheum.2012.153.
[2] S. Tanaka, Emerging anti-osteoclast therapy for rheumatoid arthritis, J. Orthop. Sci. 23 (2018) 717–721, https://doi.org/10.1016/j.jos.2018.06.001.
[3] D.S. Amarasekara, H. Yun, S. Kim, N. Lee, H. Kim, J. Rho, Regulation of osteoclast differentiation by cytokine networks, Immune Netw 18 (2018) e8, https://doi.org/10.4110/in.2018.18.e8.
[4] Q. Gu, H. Yang, Q. Shi, Macrophages and bone inflammation, J. Orthop. Transl. 10 (2017) 86–93, https://doi.org/10.1016/j.jot.2017.05.002.
[5] J.H. Kim, N. Kim, Signaling pathways in osteoclast differentiation, Chonnam Med. J. 52 (2016) 12–17, https://doi.org/10.4068/cmj.2016.52.1.12.
[6] B.F. Boyce, L. Xing, Functions of RANKL/RANK/OPG in bone modeling and remodeling, Arch. Biochem. Biophys. 473 (2008) 139–146, https://doi.org/10.1016/j.abb.2008.03.018.
[7] A. Bernhardt, K. Koperski, M. Schumacher, M. Gelinsky, Relevance of osteoclast-specific enzyme activities in cell-based in vitro resorption assays, Eur. Cell. Mater. 33 (2017) 28–42, https://doi.org/10.22203/eCM.v033a03.
[8] H. Hase, Y. Kanno, H. Kojima, D. Sakurai, T. Kobata, Coculture of osteoclast precursors with rheumatoid synovial fibroblasts induces osteoclastogenesis via transforming growth factor beta-mediated down-regulation of osteoprotegerin, Arthritis Rheum. 58 (2008) 3356–3365, https://doi.org/10.1002/art.23971.
[9] A.Y. Ng, C. Tu, S. Shen, D. Xu, M.J. Oursler, J. Qu, S. Yang, Comparative characterization of osteoclasts derived from murine bone marrow macrophages and RAW 264.7 cells using quantitative proteomics, JBMR Plus 2 (2018) 328–340, https://doi.org/10.1002/jbm4.10058.
[10] M.M. Matzelle, M.A. Gallant, K.W. Condon, N.C. Walsh, C.A. Manning, G.S. Stein, J.B. Lian, D.B. Burr, E.M. Gravallese, Resolution of inflammation induces osteoblast function and regulates the Wnt signaling pathway, Arthritis Rheum. 64 (2012) 1540–1550, https://doi.org/10.1002/art.33504.
[11] G. Schett, J. Zwerina, J.-P. David, The role of Wnt proteins in arthritis, Nat. Clin. Pract. Rheumatol. 4 (2008) 473–480, https://doi.org/10.1038/ncprheum0881.
[12] Y. Liu, F.-M. Song, S.-T. Ma, A. Moro, W.-Y. Feng, S.-J. Liao, X.-X. Lin, J.-M. Zhao, Z.-Y. Wang, J. Xu, X.-L. Zhan, Q. Liu, Vaccarin prevents titanium particle-induced osteolysis and inhibits RANKL-induced osteoclastogenesis by blocking NF-kappaB and MAPK signaling pathways, J. Cell. Physiol. (2019), https://doi.org/10.1002/jcp.28063.
[13] H.D. Jang, J.H. Shin, D.R. Park, J.H. Hong, K. Yoon, R. Ko, C.-Y. Ko, H.-S. Kim, D. Jeong, N. Kim, S.Y. Lee, Inactivation of glycogen synthase kinase-3beta is required for osteoclast differentiation, J. Biol. Chem. 286 (2011) 39043–39050, https://doi.org/10.1074/jbc.M111.256768.
[14] J.B. Moon, J.H. Kim, K. Kim, B.U. Youn, A. Ko, S.Y. Lee, N. Kim, Akt induces osteoclast differentiation through regulating the GSK3beta/NFATc1 signaling cascade, J. Immunol. 188 (2012) 163–169, https://doi.org/10.4049/jimmunol.1101254.
[15] S. Medunjanin, L. Schleithoff, C. Fiegehenn, S. Weinert, W. Zuschratter, R.C. Braun-dullaeus, GSK-3 β Controls NF-kappaB Activity Via IKK γ/NEMO, (2016), pp. 1–11, https://doi.org/10.1038/srep38553.
[16] Y.-X. Zhou, L.-X. Shi, H. Yang, Y.-G. Long, L.U. Meng, L.-S. Lv, Y. Zhang, H. Yao, L. Li, Y.-N. Yu, Effects of a GSK-3beta inhibitor on the renal expression levels of RANK, RANKL and NF-kappaB in a rat model of diabetic nephropathy, Exp. Ther. Med. 11 (2016) 2495–2502, https://doi.org/10.3892/etm.2016.3184.
[17] J. Shin, H. Jang, J. Lin, S.Y. Lee, PKC beta positively regulates RANKL-induced osteoclastogenesis by inactivating GSK-3beta, Mol. Cells. 37 (2014) 747–752, https://doi.org/10.14348/molcells.2014.0220.
[18] C. Miao, Y. Yang, X. He, X. Li, C. Huang, Y. Huang, L. Zhang, X.-W. Lv, Y. Jin, J. Li, Wnt signaling pathway in rheumatoid arthritis, with special emphasis on the different roles in synovial inflammation and bone remodeling, Cell. Signal. 25 (2013) 2069–2078, https://doi.org/10.1016/j.cellsig.2013.04.002.
[19] M. Amirhosseini, R.V. Madsen, K.J. Escott, M.P. Bostrom, F.P. Ross, A. Fahlgren, GSK-3beta inhibition suppresses instability-induced osteolysis by a dual action on osteoblast and osteoclast differentiation, J. Cell. Physiol. 233 (2018) 2398–2408, https://doi.org/10.1002/jcp.26111.

[20] S.J. Wimalawansa, Prevention and treatment of osteoporosis: efficacy of combination of hormone replacement therapy with other antiresorptive agents, J. Clin. Densitom. 3 (2) (2000) 187–201.
[21] S. Zaheer, M. LeBoff, E.M. Lewiecki, Denosumab for the treatment of osteoporosis, Expert Opin. Drug Metab. Toxicol. 11 (3) (2015) 461–470.
[22] J. An, D. Hao, Q. Zhang, B. Chen, R. Zhang, Y. Wang, H. Yang, Natural products for treatment of bone erosive diseases: the effects and mechanisms on inhibiting osteoclastogenesis and bone resorption, Int. Immunopharmacol. 36 (2016) 118–131.
[23] X. Wang, X. He, C.-F. Zhang, C.-R. Guo, C.-Z. Wang, C.-S. Yuan, Anti-arthritic effect of berberine on adjuvant-induced rheumatoid arthritis in rats, Biomed. Pharmacother. 89 (2017) 887–893, https://doi.org/10.1016/j.biopha.2017.02.099.
[24] Z. Wang, Z. Chen, S. Yang, Y. Wang, Z. Huang, J. Gao, S. Tu, Z. Rao, Berberine ameliorates collagen-induced arthritis in rats associated with anti-inflammatory and anti-angiogenic effects, Inflammation 37 (2014) 1789–1798, https://doi.org/10.1007/s10753-014-9909-y.
[25] P. Ganova, V. Gyurkovska, N. Ivanovska, Berberine influences bone homeostasis through inhibited osteoclastogenesis in zymosan-induced model of rheumatoid arthritis, Immunome.Res 12 (Suppl) (2016) 3.
[26] X. Xie, W. Li, T. Lan, W. Liu, J. Peng, K. Huang, J. Huang, Berberine Ameliorates Hyperglycemia in Alloxan-induced Diabetic C57BL/6 Mice through Activation of Akt Signaling Pathway, 58 (2011), pp. 761–768.
[27] F.-Y. Yu, C.-Q. Xie, J.-T. Sun, W. Peng, X.-W. Huang, Overexpressed miR-145 inhibits osteoclastogenesis in RANKL-induced bone marrow-derived macrophages and ovariectomized mice by regulation of Smad3, Life Sci. 202 (2018) 11–20, https://doi.org/10.1016/j.lfs.2018.03.042.
[28] C. Shi, J. Qi, P. Huang, M. Jiang, Q. Zhou, H. Zhou, H. Kang, N. Qian, Q. Yang, L. Guo, L. Deng, MicroRNA-17/20a inhibits glucocorticoid-induced osteoclast differentiation and function through targeting RANKL expression in osteoblast cells, Bone 68 (2014) 67–75, https://doi.org/10.1016/j.bone.2014.08.004.
[29] Y. Lee, H.J. Kim, C.K. Park, Y.-G. Kim, H.-J. Lee, J.-Y. Kim, H.-H. Kim, MicroRNA-124 regulates osteoclast differentiation, Bone 56 (2013) 383–389, https://doi.org/10.1016/j.bone.2013.07.007.
[30] C. Dou, C. Zhang, F. Kang, X. Yang, H. Jiang, Y. Bai, J. Xiang, J. Xu, S. Dong, MiR-7b directly targets DC-STAMP causing suppression of NFATc1 and c-Fos signaling during osteoclast fusion and differentiation, Biochim. Biophys. Acta 1839 (2014) 1084–1096, https://doi.org/10.1016/j.bbagrm.2014.08.002.
[31] N. Wang, M. Zhu, X. Wang, H.-Y. Tan, S.-W. Tsao, Y. Feng, Berberine-induced tumor suppressor p53 up-regulation gets involved in the regulatory network of MIR-23a in hepatocellular carcinoma, Biochim. Biophys. Acta 1839 (2014) 849–857, https://doi.org/10.1016/j.bbagrm.2014.05.027.
[32] J. Hu, C. Zhai, J. Hu, Z. Li, H. Fei, Z. Wang, W. Fan, MiR-23a inhibited IL-17-mediated proinflammatory mediators expression via targeting IKKalpha in articular chondrocytes, Int. Immunopharmacol. 43 (2017) 1–6, https://doi.org/10.1016/j.intimp.2016.11.031.
[33] M. Jia, C. Deng, J. Luo, P. Zhang, X. Sun, Z. Zhang, T. Gong, A novel dexamethasone-loaded liposome alleviates rheumatoid arthritis in rats, Int. J. Pharm. 540 (2018) 57–64, https://doi.org/10.1016/j.ijpharm.2018.02.001.
[34] S. Ghosh, B. Mukherjee, S. Chaudhuri, T. Roy, A. Mukherjee, S. Sengupta, Methotrexate Aspasomes against rheumatoid arthritis: optimized hydrogel loaded liposomal formulation with in vivo evaluation in Wistar rats, AAPS PharmSciTech 19 (2018) 1320–1336, https://doi.org/10.1208/s12249-017-0939-2.
[35] P.L. Van Lent, A.E. Holthuysen, N. Van Rooijen, L.B. Van De Putte, W.B. Van Den Berg, Local removal of phagocytic synovial lining cells by clodronate-liposomes decreases cartilage destruction during collagen type II arthritis, Ann. Rheum. Dis. 57 (1998) 408–413, https://doi.org/10.1136/ard.57.7.408.
[36] S. Morishima, I. Morita, T. Tokushima, H. Kawashima, M. Miyasaka, K. Omura, S. Murota, Expression and role of mannose receptor/terminal high-mannose type oligosaccharide on osteoclast precursors during osteoclast formation, J. Endocrinol. 176 (2003) 285–292.
[37] F. Sultana, M.K. Neog, M. Rasool, Targeted delivery of morin, a dietary bioflavanol encapsulated mannosylated liposomes to the macrophages of adjuvant-induced arthritis rats inhibits inflammatory immune response and osteoclastogenesis, Eur. J. Pharm. Biopharm. 115 (2017) 229–242, https://doi.org/10.1016/j.ejpb.2017.03.009.
[38] M.K. Neog, M. Rasool, Targeted delivery of p-coumaric acid encapsulated mannosylated liposomes to the synovial macrophages inhibits osteoclast formation and bone resorption in the rheumatoid arthritis animal model, Eur. J. Pharm. Biopharm. 133 (2018) 162–175, https://doi.org/10.1016/j.ejpb.2018.10.010.
[39] F. Sultana, M.K. Neog, M. Rasool, Withaferin-A, a steroidal lactone encapsulated mannose decorated liposomes ameliorates rheumatoid arthritis by intriguing the macrophage repolarization in adjuvant-induced arthritic rats, Colloids Surf. B. Biointerfaces. 155 (2017) 349–365, https://doi.org/10.1016/j.colsurfb.2017.04.046.
[40] S. Kwok, M. Cho, M. Park, H. Oh, J. Park, Y. Her, et al., Interleukin-21 promotes osteoclastogenesis in humans with rheumatoid arthritis and in mice with collagen induced arthritis, Arthritis Rheum. 64 (2012) 740–751.
[41] Y.B. Li, P. Xu, K. Xu, Y.S. Cai, M.Y. Sun, L. Yang, J. Sun, S.-M. Lu, Methotrexate affects HMGB1 expression in rheumatoid arthritis, and the downregulation of HMGB1 prevents rheumatoid arthritis progression, Mol. Cell. Biochem. 420 (2016) 161–170, https://doi.org/10.1007/s11010-016-2783-1.
[42] S. Sujitha, P. Dinesh, M. Rasool, Berberine modulates ASK1 signaling mediated through TLR4/TRAF2 via upregulation of miR-23a, Toxicol. Appl. Pharmacol. 359 (2018) 34–46, https://doi.org/10.1016/j.taap.2018.09.017.
[43] M. Vishal, S. Vimalraj, R. Ajeetha, M. Gokulnath, R. Keerthana, Z. He, N.C. Partridge, N. Selvamurugan, MicroRNA-590-5p stabilizes Runx2 by targeting Smad7 during osteoblast differentiation, J. Cell. Physiol. 232 (2017) 371–380, https://doi.org/10.1002/jcp.25434.
[44] S. Aslani, A. Abhari, E. Sakhinia, D. Sanajou, H. Rajabi, S. Rahimzadeh, Interplay between microRNAs and Wnt, transforming growth factor-beta, and bone morphogenic protein signaling pathways promote osteoblastic differentiation of mesenchymal stem cells, J. Cell. Physiol. (2018), https://doi.org/10.1002/jcp.27582.
[45] S. Wan, X. Chen, Y. He, X. Yu, Novel functions of MicroRNA-17-92 cluster in the endocrine system, Curr. Drug Targets 19 (2018) 191–200, https://doi.org/10.2174/1389450118666171117125319.
[46] J. Park, S. Wada, T. Ushida, T. Akimoto, The microRNA-23a has limited roles in bone formation and homeostasis in vivo, Physiol. Res. 64 (2015) 711–719.
[47] Y. Niwa, S. Yamada, F. Sonohara, K. Kurimoto, M. Hayashi, M. Tashiro, N. Iwata, M. Kanda, C. Tanaka, D. Kobayashi, G. Nakayama, M. Koike, M. Fujiwara, Y. Kodera, Identification of a serum-based miRNA signature for response of esophageal squamous cell carcinoma to neoadjuvant chemotherapy, J. Transl. Med. 17 (1) (2019), https://doi.org/10.1186/s12967-018-1762-6.
[48] K. Yachi, M. Tsuda, S. Kohsaka, L. Wang, Y. Oda, S. Tanikawa, Y. Ohba, S. Tanaka, miR-23a promotes invasion of glioblastoma via HOXD10-regulated glial-mesenchymal transition, Signal Transduct. Target. Ther. 3 (2018) 33, , https://doi.org/10.1038/s41392-018-0033-6.
[49] H. Luo, Y. Han, J. Liu, Y. Zhang, Identification of microRNAs in granulosa cells from patients with different levels of ovarian reserve function and the potential regulatory function of miR-23a in granulosa cell apoptosis, Gene 686 (2019) 250–260, https://doi.org/10.1016/j.gene.2018.11.025.
[50] Q. Guo, Y. Chen, L. Guo, T. Jiang, Z. Lin, miR-23a/b regulates the balance between osteoblast and adipocyte differentiation in bone marrow mesenchymal stem cells, Bone Res 4 (2016) 16022, , https://doi.org/10.1038/boneres.2016.22.
[51] H.-C. Zeng, Y. Bae, B.C. Dawson, Y. Chen, T. Bertin, E. Munivez, P.M. Campeau, J. Tao, R. Chen, B.H. Lee, MicroRNA miR-23a cluster promotes osteocyte differentiation by regulating TGF-beta signalling in osteoblasts, Nat. Commun. 8 (2017) 15000, , https://doi.org/10.1038/ncomms15000.
[52] Y. Gindin, Y. Jiang, P. Francis, R.L. Walker, O.D. Abaan, Y.J. Zhu, P.S. Meltzer, miR-23a impairs bone differentiation in osteosarcoma via down-regulation of GJA1, Front. Genet. 6 (2015) 233, https://doi.org/10.3389/fgene.2015.00233.
[53] H. Liu, R. Zhu, L. Wang, C. Liu, R. Ma, B. Qi, B. Chen, L. Li, Y. Guo, S. Shi, Q. Jia, J. Niu, D. Zhao, F. Mo, S. Gao, D. Zhang, Radix Salviae miltiorrhizae improves bone microstructure and strength through Wnt/beta-catenin and osteoprotegerin/receptor activator for nuclear factor-kappaB ligand/cathepsin K signaling in ovariectomized rats, Phytother. Res. 32 (2018) 2487–2500, https://doi.org/10.1002/ptr.6188.
[54] G. Chen, Q. Xu, M. Dai, X. Liu, Bergapten suppresses RANKL-induced osteoclastogenesis and ovariectomy-induced osteoporosis via suppression of NF-kappaB and JNK signaling pathways, Biochem. Biophys. Res. Commun. 509 (2019) 329–334, https://doi.org/10.1016/j.bbrc.2018.12.112.
[55] Y. Xiao, K. Li, Z. Wang, F. Fu, S. Shao, F. Song, J. Zhao, W. Chen, Q. Liu, J. Xu, Pectolinarigenin prevents bone loss in ovariectomized mice and inhibits RANKL-induced osteoclastogenesis via blocking activation of MAPK and NFATc1 signaling, J. Cell. Physiol. (2019), https://doi.org/10.1002/jcp.28079.
[56] L.D. Antika, E.-J. Lee, Y.-H. Kim, M.-K. Kang, S.-H. Park, D.Y. Kim, H. Oh, Y.-J. Choi, Y.-H. Kang, Dietary phlorizin enhances osteoblastogenic bone formation through enhancing beta-catenin activity via GSK-3beta inhibition in a model of senile osteoporosis, J. Nutr. Biochem. 49 (2017) 42–52, https://doi.org/10.1016/j.jnutbio.2017.07.014.
[57] H.D. Jang, J.Y. Noh, J.H. Shin, J.J. Lin, S.Y. Lee, PTEN regulation by the Akt/GSK-3beta axis during RANKL signaling, Bone 55 (2013) 126–131, https://doi.org/10.1016/j.bone.2013.02.005.
[58] 58 H. Huynh, Y. Wan, mTORC1 Impedes Osteoclast Differentiation Via Calcineurin and NFATc1, (n.d.). doi:https://doi.org/10.1038/s42003-018-0028-4
[59] B. Marchand, D. Arsenault, A. Raymond-Fleury, F.-M. Boisvert, M.-J. Boucher, Glycogen synthase kinase-3 (GSK3) inhibition induces prosurvival autophagic signals in human pancreatic cancer cells, J. Biol. Chem. 290 (2015) 5592–5605, https://doi.org/10.1074/jbc.M114.616714.
[60] I.E. Allijn, B.M.S. Czarny, X. Wang, S.Y. Chong, M. Weiler, A.E. da Silva, J.M. Metselaar, C.S.P. Lam, G. Pastorin, D.P.V. de Kleijn, G. Storm, J.-W. Wang, R.M. Schiffelers, Liposome encapsulated berberine treatment attenuates cardiac dysfunction after myocardial infarction, J. Control. Release 247 (2017) 127–133, https://doi.org/10.1016/j.jconrel.2016.12.042.
[61] C. Hagert, O. Sareila, T. Kelkka, S. Jalkanen, R. Holmdahl, The macrophage mannose receptor regulate Mannan-induced psoriasis, psoriatic arthritis, and rheumatoid arthritis-like disease models, Front. Immunol. 9 (2018) 114, https://doi.org/10.3389/fimmu.2018.00114.
[62] F. Fu, S. Shao, Z. Wang, F. Song, X. Lin, J. Ding, C. Li, Z. Wu, K. Li, Y. Xiao, Y. Su, J. Zhao, Q. Liu, J. Xu, Scutellarein inhibits RANKL-induced osteoclast formation in vitro and prevents LPS-induced bone loss in vivo, J. Cell. Physiol. (2018), https://doi.org/10.1002/jcp.27888.